

一例具有可逆热诱导电荷转移行为的二维氰基桥联 W^V-Co^{II} 配合物

刘丹 赵亮* 邵震 孟银杉 刘涛*

(大连理工大学, 精细化工国家重点实验室, 大连 116024)

摘要: 具有不同自旋态的磁性双稳态材料因在存储器件和分子开关领域具有广泛的应用前景而备受关注。本文报道了一种基于 W^V-Co^{II} 电荷转移过程的新型磁性双稳态化合物。通过将4-((2-萘-1-基)乙烯基)吡啶(4-nvp)引入氰基桥接的 W^V-Co^{II} 层框架中, 合成了一例氰基桥联二维双金属网络配合物 $\{[W^V(CN)_8]_2[Co^{II}(4-nvp)_4]_3\} \cdot 4CH_3OH$ (**1**), 其中辅助配体4-nvp可以提供分子内和分子间 $\pi-\pi$ 相互作用。磁性研究结果表明, 化合物**1**表现出可逆的电子转移耦合诱导自旋转变行为(ETCST)。该过程使体系自旋态由 $W^V-CN-Co^{II}_{HS}$ (HS=高自旋)变到 $W^V-CN-Co^{II}_{LS}$ (LS=低自旋), 并伴随着宽度为27 K的热迟滞。

关键词: 电子转移耦合诱导自旋转变; 氰基桥联; 二维网络结构; $\pi-\pi$ 相互作用

中图分类号: O614.61*3; O614.81*2 文献标识码: A 文章编号: 1001-4861(2023)02-0367-08

DOI: 10.11862/CJIC.2023.001

A 2D cyano-bridged W^V-Co^{II} coordination network exhibiting reversible thermal-induced charge transfer

LIU Dan ZHAO Liang* SHAO Zhen MENG Yin-Shan LIU Tao*

(State Key Laboratory of Fine Chemicals, Dalian University of Technology, Dalian, Liaoning 116024, China)

Abstract: Magnetic bistable materials featuring switchable spin states are of substantial interest in terms of their promising application in memory devices and switches. Here, we report a new magnetic bistable compound based on W^V-Co^{II} charge transfer. A 2D cyano-bridged heterobimetallic network $\{[W^V(CN)_8]_2[Co^{II}(4-nvp)_4]_3\} \cdot 4CH_3OH$ (**1**) (4-nvp=4-(2-(naphthalene-1-yl)vinyl)pyridine) is synthesized by incorporating the 4-nvp into the cyano-bridged W^V-Co^{II} layer framework to provide intra- and intermolecular $\pi-\pi$ interaction. Magnetic studies show that compound **1** exhibits a reversible electron-transfer-coupled spin transition (ETCST) with interconversion between the $W^V-CN-Co^{II}_{HS}$ (HS=high spin) and $W^V-CN-Co^{II}_{LS}$ (LS=low spin) linkages, accompanied by a thermal hysteresis with a width of about 27 K. CCDC: 2216222, **1** (120 K); 2215990, **1** (295 K).

Keywords: electron-transfer-coupled spin transition; cyano-bridged; 2D network; $\pi-\pi$ interaction

0 Introduction

Magnetic molecular switchable materials exhibiting bistable chemical and physical properties associated with the electron movement and charge redistribution under external stimuli such as temperature^[1-2], light^[3-4], electric field^[5], pressure^[6], or guest mole-

cules^[7], are attracting considerable interest for both fundamental interests and potential applications such as switching, display, sensors, information storage devices^[8-14]. Typical magnetic molecular switchable materials have been demonstrated concerning variations in electron configuration, such as spin crossover (SCO) of $3d^4-3d^7$ ions, valence tautomerism in a pair of metal

收稿日期: 2022-10-31。收修改稿日期: 2022-11-27。

国家自然科学基金(No.22103009, 22025101, 22222103, 22173015, 21871039, 21801037, 91961114, 22071017)资助。

*通信联系人。E-mail: liutao@dlut.edu.cn, zhaoliang716@dlut.edu.cn

ions, and ring-opening/closing and *cis-trans* isomerization^[15-20]. Among them, ETCST (electron-transfer-coupled spin transition) compounds have emerged as the topic issue in this field because of their excellent adjustable bistable characters deriving from the inter-converted metal - to - metal charge transfer (MMCT) between two energetically adjacent metal sites^[21-23]. In the recent decade, the MMCT process has been utilized as the switchable unit to manipulate magnetic, electric, thermal expansion, and photochromic properties^[24-25]. The most famous MMCT system is the cyano-bridged bimetallic Fe-Co Prussian blue analogues (PBAs) that were first observed by Hashimoto et al. and widely used to construct molecular-based materials with a synergistic response to multiple functions^[26-31]. Octacyano-metalate-based compounds have also been certified to be suitable systems to expand the family of ETCST materials, such as in $\text{Cu}^{\text{II}}-\text{Mo}^{\text{IV}}$, $\text{W}^{\text{V}}-\text{Co}^{\text{II}}$, and $\text{W}^{\text{V}}-\text{Fe}^{\text{II}}$ compounds involving the valence - state conversion $\text{W}^{\text{IV/V}}$ and $\text{Mo}^{\text{IV/V}}$ ^[5,32-37].

Moreover, octacyanometallate ions possessing more diffuse *4d/5d* orbitals and large spin-orbit coupling constants can produce stronger magnetic interaction with another adjacent metal ion, which will give benefit in constructing multi - responsive molecular magnets with higher Curie temperature^[3,38]. In particular, the W - Co charge - transfer compounds display appealing features in their photo-induced magnetic states, such as huge magnetic hysteresis and site-selective switching^[39-42]. However, it is still a big challenge to construct W - Co charge - transfer compounds. Until now, only a few samples have been reported, and most of them fail to obtain well-defined structures at different temperatures to confirm the occurrence of the charge-transfer process. First, it is because $[\text{W}(\text{CN})_8]^{3-}$ unit has a more flexible way to connect with Co^{II} with its eight cyano groups. As a result, it is not easy to control the coordination sphere of Co^{II} centers and the dimensions of the overall structure. Second, the occurrence of charge transfer requires the constituent Co^{II} center located at a suitable coordination environment to provide equivalent redox potential with adjacent W^{V} ions. Therefore, rational selection of the auxiliary

ligands is important. Third, the thermal hysteresis of the charge-transfer materials, which is crucial for practical application, needs suitable intermolecular interactions. With these concerns, we aim to assemble $[\text{W}(\text{CN})_8]^{3-}$ with Co^{II} to obtain a novel $\text{W}^{\text{V}}-\text{Co}^{\text{II}}$ charge-transfer compound, in which the auxiliary ligands 4-(2-naphthalene-1-yl)vinyl pyridine (4-nvp) is selected to adjust the coordination sphere of the Co^{II} center and provide intermolecular $\pi-\pi$ interaction. Herein, a 2D reticular cyano-bridge compound $\{[\text{W}^{\text{V}}(\text{CN})_8]_2[\text{Co}^{\text{II}}(4\text{-nvp})_4]_3\} \cdot 4\text{CH}_3\text{OH}$ (**1**) is reported, which underwent incomplete MMCT in a temperature range of 90-180 K with a 27 K-width thermal hysteresis.

1 Experimental

1.1 Materials

All chemicals were purchased from commercial suppliers and used without further purification. The building blocks $(\text{Bu}_4\text{N})_3[\text{W}(\text{CN})_8] \cdot 2\text{H}_2\text{O}$ (Bu_4N =tetrabutylammonium) were synthesized according to the literature.

1.2 Synthesis of 4-nvp

In a 250 mL three-necked flask, reaction mixtures of 1-bromonaphthalene (2.25 g, 10.937 mmol), 4-vinyl pyridine (1.2 mL, 11.288 mmol), tri(*o*-tolyl)phosphine (0.6 g, 1.970 mmol), $\text{Pd}(\text{OAc})_2$ (21 mg, 0.093 5 mmol), and triethylamine (60 mL) in dry DMF (30 mL) were thoroughly mixed under argon. The reaction mixture was then degassed by free-pump-thaw five times before heating at 85 °C for 12 h. After this time, the reaction mixture cooled to room temperature, and the triethylamine was removed by rotary evaporation, water (50 mL) was added. The mixture was extracted with CH_2Cl_2 (3×50 mL). Then the organic phase was extracted with H_2O (3×50 mL) and saturated NaHCO_3 (3×50 mL). The solution was dried over anhydrous MgSO_4 and concentrated under a vacuum. The crude product was purified by column chromatography (silica gel, ethyl acetate/petroleum ether, 2:1, *V/V*) and a yellow product (2.115 g, 69%) was got.

1.3 Synthesis of compound 1

Compound **1** was synthesized by diffusion method in a test tube. The aqueous solution (1.0 mL) of Co

$(ClO_4)_2 \cdot 6H_2O$ (1.83 mg, 0.005 0 mmol) was slowly added dropwise to the bottom of the test tube. Then a mixture of methanol/water (1 : 1, *V/V*, 3 mL) was layered as the middle buffer. Finally, 1.0 mL methanol solution of $(Bu_4N)_3[W(CN)_8]$ (0.010 mmol) and 4-nvp (0.010 mmol) was carefully added as the third layer. After a few weeks, black red crystals were collected (Yield: 1.23 mg, 19% based on $Co(ClO_4)_2 \cdot 6H_2O$). Anal. Calcd. for $C_{224}H_{172}Co_3W_2N_{28}O_4$ (%): C 69.73, H 4.46, N 10.17; Found(%): C 69.81, H 4.45, N 10.20.

1.4 Physical measurement

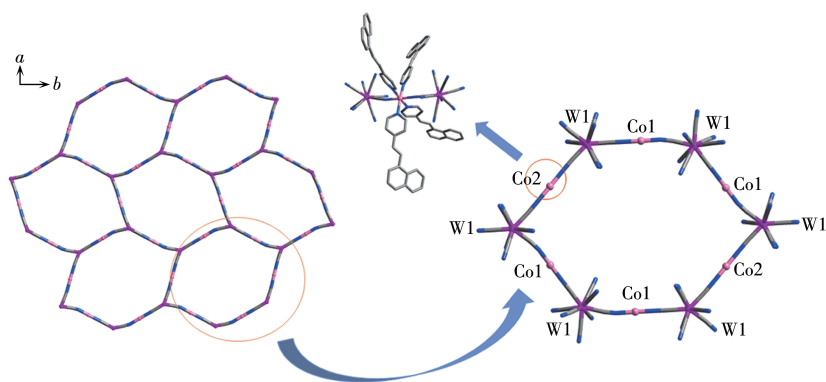
The single-crystal X-ray diffraction data for **1** were collected on a Bruker D8 Venture CMOS-based diffractometer (Mo $K\alpha$ radiation, $\lambda = 0.071\ 073$ nm) using the SMART and SAINT programs. Final unit cell parameters were based on all observed reflections from the integration of all frame data. The structures were solved with the ShelXT structure solution program using Intrinsic Phasing and refined with the ShelXL refinement package using Least Squares minimization that was implanted in Olex2. The powder X-ray diffraction (PXRD) patterns were collected on a Rigaku Smartlab 9 kW X-ray diffractometer (Cu $K\alpha$ radiation, $\lambda = 0.154\ 178$ nm, $U = 45$ kV, $I = 200$ mA) in a range of $5^\circ - 50^\circ$ at a rate of $5^\circ \cdot \text{min}^{-1}$. Variable-temperature infrared spectra were measured on KBr pellet samples using a Nicolet iS10 FT-IR spectrometer equipped with a Bruker cryostat (Optistat CF2). UV-Vis absorption spectra were recorded on a HITACHI UH-4150 UV-Vis spectrophotometer. Magnetic measurement of the sample was performed on a PPMS magnetometer. Data

were corrected for the diamagnetic contribution calculated from Pascal constants. The sample (12.85 mg) was measured under a DC field of 1 000 Oe. The variable-temperature magnetization data were collected within a temperature range of 2-300 K at a rate of $2\ \text{K} \cdot \text{min}^{-1}$. The elemental analysis was performed by Elemental Vario EL III (Germany). Thermogravimetric analysis was performed under an N_2 atmosphere at $10\ \text{K} \cdot \text{min}^{-1}$ using a TG/DTA STD-Q600 system (TA Instruments, the United States).

2 Results and discussion

2.1 Crystal structure

Compound **1** was synthesized by the diffusion method through the reaction of $Co(ClO_4)_2 \cdot 6H_2O$, 4-nvp, and $(Bu_4N)_3[W(CN)_8] \cdot 2H_2O$ in a methanol/water mixture, and the crystals were obtained after a few weeks. Single-crystal X-ray diffraction analysis at 120 K revealed that **1** crystallizes in a monoclinic space group $P2_1/n$ (Table S1, Supporting information). The unit cell consists of two $[W(CN)_8]^{3-}$ units and three $[Co(4-nvp)_4]^{2+}$ units, forming a wavy-like layer connected by CN^- bond along the *a*-axis and *c*-axis (Fig.S1-S3). The layer is constituted with alternately W^V and Co^{II} ions through cyano groups, presenting a hexagonal grid structure arranged in order (Fig.1). In the layers, each $[W(CN)_8]^{3-}$ unit bridges three Co^{II} ions through three of its eight CN^- groups, and each Co^{II} ion is coordinated to two nitrogen atoms from the cyanide ligand in the apical positions and four nitrogen atoms from the 4-nvp ligand in the equatorial positions. The coordination



W: purple, Co: pink, C: gray, N: blue, O: red; The H atom and methanol molecules are omitted for clarity

Fig.1 Arrangement of **1** in the *ab* plane (left) and detailed structural linkage (right)

Table 1 Selected bond lengths (nm) and bond angles ($^{\circ}$) of **1** at 120 and 295 K, respectively

Bond length / angle	120 K	295 K
Co1—N1	0.190 6(6)	0.213 8(4)
Co1—N2	0.189 1(6)	0.215 1(4)
Co1—N3	0.196 7(6)	0.215 8(4)
Co1—N4	0.195 9(6)	0.214 8(5)
Co1—N5	0.198 0(6)	0.217 4(5)
Co1—N6	0.198 0(6)	0.217 3(5)
Co1—N _{avg}	0.194 7(1)	0.215 7(0)
Co2—N12	0.214 7(6)	0.214 5(5)
Co2—N13	0.218 0(8)	0.215 9(8)
Co2—N14	0.218 6(10)	0.220 8(10)
Co2—N _{avg}	0.217 1(0)	0.217 0(6)
W1—C _{avg}	0.216 7(7)	0.216 3(3)
\angle Co1—N \equiv C	170.4(6)	166.1(4)
\angle Co2—N \equiv C	179.1(7)	176.9(6)

geometry of the W and Co^{II} site were square antiprism (D_{4d}) and octahedron (O_h), respectively. Two free water molecules were located around $[\text{W}(\text{CN})_8]^{3-}$, forming hydrogen bonds with the uncoordinated CN^- ligands as hydrogen bond lengths of 0.192 1 and 0.201 6 nm ($\text{H}\cdots\text{O}$), respectively (Fig.S4). The nearest metal-metal distance between the two layers is 1.763 9 nm.

At 295 K, the Co—N_{cyanide} and Co—N_{4-nvp} bond distances are 0.213 8(4)-0.215 1(4) and 0.214 8(5)-0.217 4(5) nm, respectively, which are characteristic of the high spin (HS) Co^{II} ions. The angles of Co—N \equiv C are 166.1(4) $^{\circ}$ - 176.9(6) $^{\circ}$, departing from linearity slightly. The average distances of the W—C bond are 0.216 3(3) nm, and the angles of W—N \equiv C are close to 180 $^{\circ}$. Three independent Co—W—Co angles are 137.0(2) $^{\circ}$, 136.7(3) $^{\circ}$, and 81.5(3) $^{\circ}$, respectively. When the temperature declined to 120 K, Co1—N_{cyanide} and Co1—N_{4-nvp} bond distances are shortened to 0.189 1(6)-0.190 6(6) and 0.195 9(6)-0.198 0(6) nm, respectively, whereas Co2—N_{cyanide} and Co2—N_{4-nvp} bond lengths remain unchanged, which indicate Co1^{II}_{HS} ions change into Co1^{III}_{LS} (LS=low spin). Moreover, Co1—N \equiv C and Co2—N \equiv C angles decrease by 4.3(2) $^{\circ}$ and 2.2(1) $^{\circ}$ to 170.4(6) $^{\circ}$ and 179.1(7) $^{\circ}$, respectively (Table S1 - S4). These structural characteristics variations and charge compensation indicate the occurrence of the charge

transfer between Co1^{II} and W^V ions, and **1** underwent a metal-to-metal charge-transfer from the paramagnetic W^V—CN—Co1^{II}_{HS} linkage to the diamagnetic W^{IV}—CN—Co1^{III}_{LS} linkage.

The π - π interaction is crucial not only in controlling the assembly or packing of the structure but also in manipulating the properties of the compound. The usual π - π interaction is an offset or slipped stacking of the benzene rings or aromatic nitrogen heterocycles, and the effective distance is 0.330 0-0.380 0 nm. In the layer of compound **1**, two kinds of the π - π interaction are observed between the naphthalene ring of 4-nvp molecules belonging to the Co1 and Co1 site, and Co1 and Co2 site, with the distance of 0.344 8 and 0.329 9 nm, respectively (Fig. S5). The distances between the ligands among adjacent layers are in a range of 0.363 8 to 0.371 8 nm (Fig.S6), which is in the normal range of the π - π interaction. Those observed π - π interactions directly affect the coordination mode of W—C \equiv N—Co. The sum of the angles of the three independent Co—W—Co angles is 355.2 $^{\circ}$, close to 360 $^{\circ}$. As a result, the plane only fluctuates slightly. For the PXRD analysis, the comparison of the powdered sample of **1** with the simulated pattern calculated by the single crystal structure proves that the single crystal and powder samples had the same crystallographic structure, so we used the polycrystalline sample for the next test (Fig.S6).

2.2 Spectroscopic analysis

The solid-state FT-IR spectroscopy provides further evidence for thermo-induced charge transfer. The spectrum of **1** was recorded in a range of 80-300 K, showing an explicit temperature dependence (Fig. 2a). IR peaks caused by CN^- stretching patterns were observed at 2 000 - 2 300 cm^{-1} . At low temperatures, four peaks due to the cyanide stretching vibrations were observed: 2 166, 2 160, 2 140, and 2 120 cm^{-1} , where the peaks centered at 2 120 and 2 140 cm^{-1} can be attributed to $[\text{W}^{\text{IV}}(\text{CN})_8]^{4-}$ unit. As the temperature gradually rose, these peaks gradually diminished and finally disappeared, thus confirming the thermally-induced conversion of W^{IV} to W^V. Variable-temperature solid-state UV-Vis-NIR absorption spectra of **1**

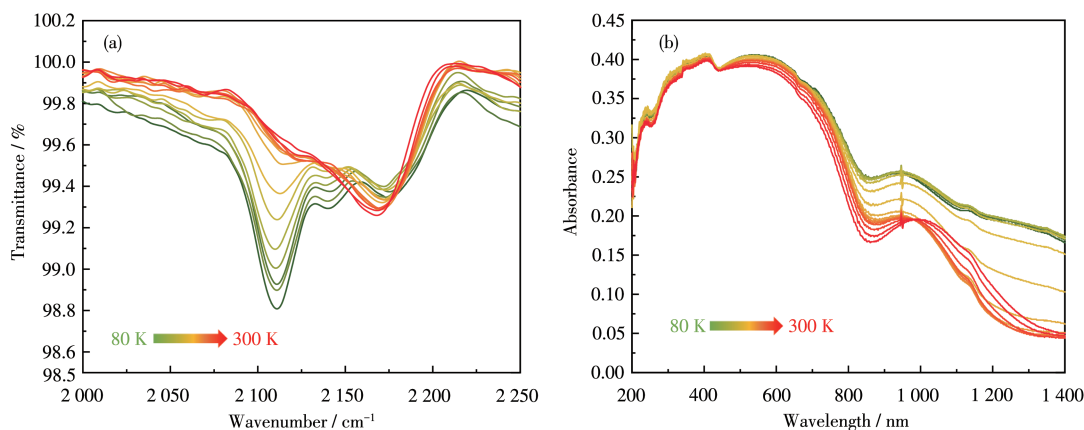


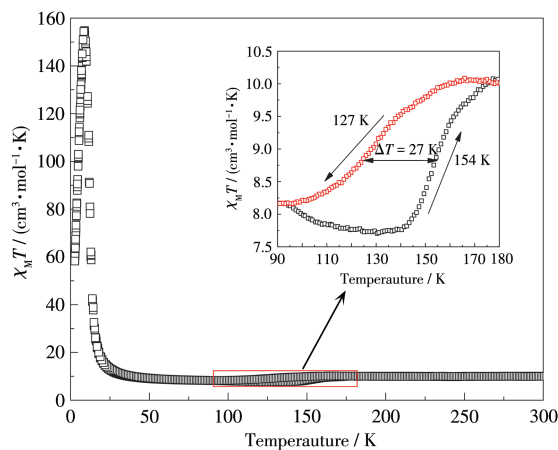
Fig.2 (a) Variable-temperature solid-state FT-IR spectra for **1**; (b) Variable-temperature solid-state UV-Vis-NIR absorption spectra for **1**

were also performed in the temperature interval of 80–300 K to further investigate the charge-transfer process. As the temperature decreased, the broad absorption bands in the region of 800–1 000 nm for the characteristic band of the $W^{IV} \rightarrow Co^{III}$ MMCT gradually increased, which demonstrates the occurrence of the charge transfer from W^V ions to Co^{II} ions (Fig.2b and S7).

2.3 Magnetic property

The temperature-dependent magnetic susceptibility measurement of **1** was measured from 2 to 300 K under the direct current (DC) field of 1 000 Oe (Fig.3). At 300 K, the $\chi_M T$ per $[Co_3W_2]$ unit was $10.03 \text{ cm}^3 \cdot \text{mol}^{-1} \cdot \text{K}$ (χ_M is the molar magnetic susceptibility), which was higher than the expected spin-only value for two isolated W^V ($S=1/2$, $g=2.04$) and three Co^{II} ($S=3/2$, $g=2.04$) due to the orbital contributions of Co^{II} ions. Upon cooling, the $\chi_M T$ remained nearly constant until 180 K and then gradually decreased to $8.16 \text{ cm}^3 \cdot \text{mol}^{-1} \cdot \text{K}$ at 90 K with $T_{1/2} \downarrow = 127 \text{ K}$. When heating the sample, the $\chi_M T$ could return to the initial value with $T_{1/2} \uparrow = 154 \text{ K}$, which represents a reversible, thermally induced charge-transfer process with a 27 K-wide thermal hysteresis. The transfer ratio was about 26.4%, which is probably attributed to the limited deformation of the coordination configuration of Co ions caused by the weak intra- and intermolecular $\pi-\pi$ interactions of **1**. Further cooling, the $\chi_M T$ gradually increased and got a sharp maximum of $161.35 \text{ cm}^3 \cdot \text{mol}^{-1} \cdot \text{K}$ at 9 K, which confirms the strong ferromagnetic interaction between

W^V and Co^{II} center. Subsequently, the $\chi_M T$ dropped sharply to $58.25 \text{ cm}^3 \cdot \text{mol}^{-1} \cdot \text{K}$ at 3.7 K due to zero-field splitting and/or antiferromagnetic interactions. This magnetic behavior determines a reversible charge-transfer process that involves conversion between the high-temperature (HT) phase with W^V ($S=1/2$)- Co^{II}_{HS} ($S=3/2$) linkage and the low-temperature (LT) phase with diamagnetic W^{IV} ($S=0$)- Co^{III}_{LS} ($S=0$) linkage. Taking into account the change in the $\chi_M T$ values, only one pair of $W^V-Co^{II}_{HS}$ linkage converted to $W^{IV}-Co^{III}_{LS}$, in accordance with the result of the crystallographic analysis. Therefore, the transformation could be expressed as $\{[W^V(CN)_{8,12}][Co^{II}_{HS}(4-nvp)_{4,13}]\} \cdot 4CH_3OH \rightarrow \{[W^V(CN)_8][W^{IV}(CN)_8][Co^{II}_{HS}(4-nvp)_4]_2[Co^{III}_{LS}(4-nvp)_4]\} \cdot 4CH_3OH$.



Inset: temperature-dependent magnetic susceptibilities of **1** in a temperature range of 90–180 K

Fig.3 Temperature-dependent magnetic susceptibilities of **1** in a temperature range of 2–300 K under an applied field of 1 000 Oe

The field-dependent magnetization of **1** was measured up to 50 kOe at 2 K (Fig.S8). The magnetization in the low field region increased rapidly to $4N\beta$ at 150 Oe, then gradually increased to $6.6N\beta$ at 50 kOe without saturation. To further investigate the change of susceptibility with the applied magnetic field, a complete hysteresis loop was recorded at 2 K, in which a subtle hysteresis was observed with a remnant magnetization (M_r) of $4.15N\beta$ and a coercive field (H_c) of 250 Oe. Zero-field-cooled (ZFC) and field-cooled (FC) magnetization of **1** were measured at 10 Oe in a temperature range of 2-20 K to investigate the phase transformation at low temperatures (Fig. S9). The ZFC and FC curves were irreversible at 9 K, which indicates the presence of spontaneous magnetization of **1** below 9 K. According to all the magnetic analysis mentioned above, we can conclude that only one $W^V - Co^{II}_{HS}$ linkage in the $[Co_3W_2]$ unit undergo charge-transfer to convert to $W^{IV} - Co^{III}_{LS}$ and the remanent $W^V - Co^{II}_{HS}$ linkage exhibit strong ferromagnetic coupling. However, no obvious photo-respond magnetic behavior of **1** has been observed at low temperatures because less distortion of the inner coordination sphere of the Co^{III}_{LS} center results in the

fast relaxation speed from the photo-induced excited state to the ground state.

To date, the report of $W^V - Co^{II}$ charge-transfer compounds is very limited. Here, we summarize four cases of related $W^V - Co^{II}$ charge-transfer compounds in the literature to discover some instructive laws for further investigation. As shown in Table 2, firstly, both 2D and 3D compounds exhibited obvious thermal hysteresis, whereas zero-dimensional (0D) clusters did not. Moreover, the width of hysteresis in 3D compounds was far broad than that of 2D ones. First, in general, thermal hysteresis is attributed to intermolecular interactions (interactions at transition sites) such as hydrogen bonding interaction and $\pi - \pi$ interaction. Therefore, to construct bistable molecules with hysteresis, the intermolecular interaction sites must be appropriately increased. Second, the cyanide-bridged $W^V - Co^{II}$ compounds with 2D and 3D configurations show large magnetic hysteresis than 0D ones, attributed to strong ferromagnetic interaction and axis anisotropy of the compound. In a multidimensional structure, numerous metal sites could support stronger interactions and systematic axial anisotropy, resulting in magnetic hystere-

Table 2 W-Co metal-metal charge transfer compounds and related structure parameters

Compound	State	Configuration	$T_{1/2}$ and ΔT	At low temperatures			At high temperatures		
				Co—N _{avg}	Σ_{Co}^a	CShM _{Co}^b}	Co—N _{avg}	Σ_{Co}	CShM _{Co}}
1	Crystal	2D	$T_{1/2} \downarrow = 127$ K	0.194 7	15.5	0.092	0.215 7	20.44	0.122
			$T_{1/2} \uparrow = 154$ K	0.217 1	20.33	0.154	0.217 0	23.2	0.154
			$\Delta T = 27$ K	0.193 1	25.8	0.175 0	0.213 0	33.4	0.215
[Co(bik) ₃][W(CN) ₈] ₃ {Co-(bik) ₂] ₃ ·2H ₂ O· 13CH ₃ CN ^[44]	Crystal	0D	$T_{1/2} = 215$ K	0.192 4	19.1	0.107 1	0.211 1	34.8	0.229
				0.191 2	14.8	0.057 2	0.191 2	15.0	0.054
				0.212 1	38.5	2.226 3	0.213 1	38.0	0.267
Cs ⁺ [(Co ^{II} (3-cyanopyridine) ₂] ₂ {W ^V (CN) ₈ }]· H ₂ O ^[32]	Powder	2D	$T_{1/2} \downarrow = 167$ K	—	—	—	0.210 1	11.308	0.031
			$T_{1/2} \uparrow = 216$ K	—	—	—	0.210 8	11.9	0.043
			$\Delta T = 49$ K	—	—	—	0.216 5	18.8	0.139
[(Co ^{II} (pyrimidine) ₂] ₂ {Co ^{II} (H ₂ O) ₂ }{W ^V (CN) ₈ }] ₂ · 4H ₂ O ^[39]	Powder	3D	$T_{1/2} \downarrow = 208$ K	—	—	—	0.213 1	44.455	0.033
			$T_{1/2} \uparrow = 298$ K	—	—	—	0.211 1	50.4	0.449
			$\Delta T = 90$ K	—	—	—	—	—	—
[(Co ^{II} (4-methylpyridine) (pyrimidine) ₂] ₂ {Co ^{II} (H ₂ O) ₂ }] {W ^V (CN) ₈ }] ₂ ·4H ₂ O ^[34]	Powder	3D	$T_{1/2} \downarrow = 172$ K	—	—	—	0.213 1	44.455	0.033
			$T_{1/2} \uparrow = 241$ K	—	—	—	0.211 1	50.4	0.449
			$\Delta T = 69$ K	—	—	—	—	—	—

^a The anomalous octahedral distortion parameter Σ around the Co^{II} ion; ^b continuous shape measure relative to the ideal octahedron of the Co^{II} center.

sis. Third, according to the \sum_{Co} and $CShM_{Co}$ before and after spin transition in the well-defined structure, we inferred that the ideal octahedral coordination sphere of the Co^{II} can stabilize the Co^{III}_{LS} state in the W^V-Co^{II} charge-transfer system. In summary, to constitute a W^V-Co^{II} charge-transfer material with large thermal and magnetic hysteresis, the auxiliary ligands are important. According to the literature, the smallest pyridine-based auxiliary ligands with $\pi-\pi$ interaction site are preferred not only for their ability to release the spatial resistance of the Co^{II} center to achieve the ideal octahedral coordination sphere of the Co^{II} but also to increase the magnetic dimension and intermolecular interaction of the compound.

3 Conclusions

We synthesized a cyano-bridged 2D layer W^V-Co^{II} compound $\{[W^V(CN)_8]_2[Co^{II}(4-nvp)_4]_3\} \cdot 4CH_3OH$ (**1**) by using 4-(2-(naphthalene-1-yl)vinyl)pyridine (4-nvp) as the auxiliary ligands. Due to the intra- and intermolecular interaction, compound **1** shows a wave-like configuration. Magnetic and spectroscopic studies manifest that the 2D network displays incomplete reversible charge-transfer behaviors with a 27 K width of thermal hysteresis associated with the intermolecular $\pi-\pi$ interaction. In addition, we summarize and analyze the published W^V-Co^{II} charge-transfer compounds and gave rough guidance to construct the new charge-transfer materials, which will help expand the number of magnetic molecular switchable materials.

Acknowledgments: This work was financially supported by the National Natural Science Foundation of China (Grants No. 22103009, 22025101, 22222103, 22173015, 21871039, 21801037, 91961114, and 22071017). Liu Tao thanks the financial support by the Fundamental Research Funds for the Central Universities of China (Grants No. PA2021GDSK0063 and PA2020GDJQ0028).

Supporting information is available at <http://www.wjhxxb.cn>

References:

- [1]Guo F S, He M, Huang G Z, Giblin S R, Billington D, Heinemann F

W, Tong M L, Mansikkamäki A, Layfield R A. Discovery of a dysprosium metallocene single-molecule magnet with two high-temperature Orbach processes. *Inorg. Chem.*, **2022**,**61**(16):6017-6025

[2]Kawamura A, Xie J, Boyn J N, Jesse K A, Mcneeece A J, Hill E A, Collins K A, Valdez-Moreira J A, Filatov A S, Kurutz J W, Mazziotti D A, Anderson J S. Reversible switching of organic diradical character via iron-based spin-crossover. *J. Am. Chem. Soc.*, **2020**,**142**(41):17670-17680

[3]Zhao L, Meng Y S, Liu Q, Sato O, Shi Q, Oshio H, Liu T. Switching the magnetic hysteresis of an $[Fe^{II}-NC-W^V]$ -based coordination polymer by photoinduced reversible spin crossover. *Nat. Chem.*, **2021**,**13**(7):698-704

[4]Zhu H L, Meng Y S, Hu J X, Oshio H, Liu T. Photoinduced magnetic hysteresis in a cyanide-bridged two-dimensional $[Mn_2W]$ coordination polymer. *Inorg. Chem. Front.*, **2022**,**9**(19):4974-4981

[5]Ohkoshi S, Tokoro H, Hozumi T, Zhang Y, Hashimoto K, Mathonière C, Bord I, Rombaut G, Verelst M, Cartier dit Moulin C, Villain F. Photoinduced magnetization in copper octacyanomolybdate. *J. Am. Chem. Soc.*, **2006**,**128**(1):270-277

[6]Pinkowicz D, Rams M, Mišek M, Kamenev K V, Tomkowiak H, Katrusiak A, Sieklucka B. Enforcing multifunctionality: A pressure-induced spin-crossover photomagnet. *J. Am. Chem. Soc.*, **2015**,**137**(27):8795-8802

[7]Xie K P, Ruan Z Y, Lyu B H, Chen X X, Zhang X W, Huang G Z, Chen Y C, Ni Z P, Tong M L. Guest-driven light-induced spin change in an azobenzene loaded metal-organic framework. *Angew. Chem. Int. Ed.*, **2021**,**60**(52):27144-27150

[8]Hicks R G. A new spin on bistability. *Nat. Chem.*, **2011**,**3**(3):189-191

[9]Dogariu A, Michael J B, Scully M O, Miles R B. High-gain backward lasing in air. *Science*, **2011**,**331**(6016):442-445

[10]Itkis M E, Chi X, Cordes A W, Haddon R C. Magneto-opto-electronic bistability in a phenalenyl-based neutral radical. *Science*, **2002**,**296**(5572):1443-1445

[11]Fujita W, Awaga K. Room-temperature magnetic bistability in organic radical crystals. *Science*, **1999**,**286**(5438):261-263

[12]Vincent R, Klyatskaya S, Ruben M, Wernsdorfer W, Balestro F. Electronic read-out of a single nuclear spin using a molecular spin transistor. *Nature*, **2012**,**488**(7411):357-360

[13]Ohkoshi S, Imoto K, Tsunobuchi Y, Takano S, Tokoro H. Light-induced spin-crossover magnet. *Nat. Chem.*, **2011**,**3**(7):564-569

[14]Mannini M, Pineider F, Sainctavit P, Danieli C, Otero E, Sciancalepore C, Talarico A M, Arrio M, Cornia A, Gatteschi D, Sessoli R. Magnetic memory of a single-molecule quantum magnet wired to a gold surface. *Nat. Mater.*, **2009**,**8**(3):194-197

[15]Pierpont C G. Studies on charge distribution and valence tautomerism in transition metal complexes of catecholate and semiquinonate ligands. *Coord. Chem. Rev.*, **2001**,**216-217**:99-125

[16]Aguiló D, Prado Y, Koumoussi E S, Mathonière C, Clérac R. Switchable Fe/Co Prussian blue networks and molecular analogues. *Chem. Soc. Rev.*, **2015**,**45**(1):203-224

[17]Ohkoshi S, Tokoro H, Hashimoto K. Temperature- and photo-

- induced phase transition in rubidium manganese hexacyanoferrate. *Coord. Chem. Rev.*, **2005**, *249*(17):1830-1840
- [18]王康杰, 李鸿庆, 孙宇辰, 王新益. 氢键桥连一维铁(III)自旋交叉化合物的合成和性质. *无机化学学报*, **2020**, *36*(6):1143-1148
WANG X Y, WANG K J, LI H Q, SUN Y C. Synthesis and properties of an iron(III) spin crossover compound with 1D chains bridged by hydrogen bonds. *Chinese J. Inorg. Chem.*, **2020**, *36*(6): 1143 - 1148
- [19]杨蕊, 张舒雅, 王润国, 孟银杉, 刘涛, 朱元元. 三联吡啶异配体对构筑单核钴(II)自旋交叉配合物的合成和磁性. *无机化学学报*, **2022**, *38*(8):1477-1486
YANG R, ZHANG S Y, WANG R G, MENG Y S, LIU T. Synthesis and magnetic properties of mononuclear cobalt (II) spin crossover complexes from complementary terpyridine ligand pairing. *Chinese J. Inorg. Chem.*, **2022**, *38*(8):1477-1486
- [20]Jiang W J, Jiao C Q, Meng Y S, Zhao L, Liu Q, Liu T. Switching single chain magnet behavior via photoinduced bidirectional metal-to-metal charge transfer. *Chem. Sci.*, **2018**, *9*(3):617-622
- [21]Weinberg D R, Gagliardi C J, Hull J F, Murphy C F, Kent C A, Westlake B C, Paul A, Ess D H, Mccafferty D G, Meyer T J. Proton-coupled electron transfer. *Chem. Rev.*, **2012**, *112*(7):4016-4093
- [22]Bernardo B, Cheyns D, Verreet B, Schaller R D, Rand B P, Giebink N C. Delocalization and dielectric screening of charge transfer states in organic photovoltaic cells. *Nat. Commun.*, **2014**, *5*(1):1-7
- [23]Akimov A V, Neukirch A J, Prezhdo O V. Theoretical insights into photoinduced charge transfer and catalysis at oxide interfaces. *Chem. Rev.*, **2013**, *113*(6):4496-4565
- [24]Meng Y S, Sato O, Liu T. Manipulating metal-to-metal charge transfer for materials with switchable functionality. *Angew. Chem. Int. Ed.*, **2018**, *57*(38):12216-12226
- [25]Mathonière C. Metal-to-Metal Electron Transfer: A powerful tool for the design of switchable coordination compounds. *Eur. J. Inorg. Chem.*, **2018**(3/4):248-258
- [26]Li D F, Clérac R, Roubeau O, Harté E, Mathonière C, Le Bris R, Holmes S M. Magnetic and optical bistability driven by thermally and photoinduced intramolecular electron transfer in a molecular cobalt-iron Prussian blue analogue. *J. Am. Chem. Soc.*, **2008**, *130*(1): 252-258
- [27]Zhang Y Z, Li D F, Clérac R, Kalisz M, Mathonière C, Holmes S M. Reversible thermally and photoinduced electron transfer in a cyano-bridged $\{\text{Fe}_2\text{Co}_2\}$ square complex. *Angew. Chem. Int. Ed.*, **2010**, *49*(22):3752-3756
- [28]Koumoussi E S, Jeon I, Gao Q, Dechambenoit P, Woodruff D N, Merzeau P, Buisson L, Jia X, Li D F, Volatron F, Mathonière C, Clérac R. Metal-to-metal electron transfer in Co/Fe Prussian blue molecular analogues: The ultimate miniaturization. *J. Am. Chem. Soc.*, **2014**, *136*(44):15461-15464
- [29]Liu T, Dong P D, Kanegawa S, Kang S, Sato O, Shiota Y, Yoshizawa K, Hayami S, Wu S, He C, Duan C Y. Reversible electron transfer in a linear $\{\text{Fe}_2\text{Co}\}$ trinuclear complex induced by thermal treatment and photoirradiation. *Angew. Chem. Int. Ed.*, **2012**, *51*(18):4367-4370
- [30]Huang W, Ma X, Sato O, Wu D Y. Controlling dynamic magnetic properties of coordination clusters via switchable electronic configuration. *Chem. Soc. Rev.*, **2021**, *50*(12):6832-6870
- [31]Liu Q, Yao N T, Sun H Y, Hu J X, Meng Y S, Liu T. Light actuated single-chain magnet with magnetic coercivity. *Inorg. Chem. Front.*, **2022**, *9*(19):5093-5104
- [32]Arimoto Y, Ohkoshi S, Zhong Z J, Seino H, Mizobe Y, Hashimoto K. Photoinduced magnetization in a two-dimensional cobalt octacyano-tungstate. *J. Am. Chem. Soc.*, **2003**, *125*(31):9240-9241
- [33]Chorazy S, Podgajny R, Nogas W, Nitek W, Koziel M, Rams M, Juszynska - Galazka E, Zukrowski J, Kapusta C, Nakabayashi K, Fujimoto T, Ohkoshi S, Sieklucka B. Charge transfer phase transition with reversed thermal hysteresis loop in the mixed - valence $\text{Fe}_9[\text{W}(\text{CN})_8]_6 \cdot x\text{MeOH}$ cluster. *Chem. Commun.*, **2014**, *50*(26):3484-3487
- [34]Ozaki N, Tokoro H, Hamada Y, Namai A, Matsuda T, Kaneko S, Ohkoshi S. Photoinduced magnetization with a high Curie temperature and a large coercive field in a Co-W bimetallic assembly. *Adv. Funct. Mater.*, **2012**, *22*(10):2089-2093
- [35]Herrera J M, Marvaud V, Verdagner M, Marrot J, Kalisz M, Mathonière C. Reversible photoinduced magnetic properties in the heptanuclear complex $[\text{Mo}^{\text{IV}}(\text{CN})_2(\text{CNCuL})_6]^{8+}$: A photomagnetic high-spin molecule. *Angew. Chem. Int. Ed.*, **2004**, *43*(41):5468-5471
- [36]Zhao L, Duan R, Zhuang P F, Zheng H, Jiao C Q, Wang J L, He C, Liu T. 12-Metal 36-membered ring based $\text{W}^{\text{V}}-\text{Co}^{\text{II}}$ layers showing spin-glass behavior. *Dalton Trans.*, **2015**, *44*(28):12613-12617
- [37]Podgajny R, Chorazy S, Nitek W, Rams M, Majcher A M, Marszałek B, Zukrowski J, Kapusta C, Sieklucka B. Co-NC-W and Fe-NC-W electron-transfer channels for thermal bistability in trimetallic $\{\text{Fe}_6\text{Co}_3[\text{W}(\text{CN})_8]_6\}$ cyanido-bridged cluster. *Angew. Chem. Int. Ed.*, **2013**, *52*(3):896-900
- [38]Ohkoshi S, Tokoro H. Photomagnetism in cyano-bridged bimetal assemblies. *Acc. Chem. Res.*, **2012**, *45*(10):1749-1758
- [39]Ohkoshi S, Hamada Y, Matsuda T, Tsunobuchi Y, Tokoro H. Crystal structure, charge-transfer-induced spin transition, and photoreversible magnetism in a cyano-bridged cobalt-tungstate bimetallic assembly. *Chem. Mater.*, **2008**, *20*(9):3048-3054
- [40]Mahfoud T, Molnár G, Bonhommeau S, Cobo S, Salmon L, Demont P, Tokoro H, Ohkoshi S, Boukheddaden K, Bousseksou A. Electric-field-induced charge-transfer phase transition: A promising approach toward electrically switchable devices. *J. Am. Chem. Soc.*, **2009**, *131*(41):15049-15054
- [41]Ohkoshi S, Ikeda S, Hozumi T, Kashiwagi T, Hashimoto K. Photoinduced magnetization with a high Curie temperature and a large coercive field in a cyano-bridged cobalt-tungstate bimetallic assembly. *J. Am. Chem. Soc.*, **2006**, *128*(16):5320-5321
- [42]Mondal A, Chamoreau L, Li Y, Journaux Y, Seuleiman M, Lescouëzec R. W-Co discrete complex exhibiting photo- and thermo-induced magnetisation. *Chem.-Eur. J.*, **2013**, *19*(24):7682-7685